Chemical Engineering Journal 97 (2004) 103–114

Chemical Engineering Journal

www.elsevier.com/locate/cej

Power consumption and solid suspension performance of large-scale impellers in gas–liquid–solid three-phase stirred tank reactors

N. Dohi [a], T. Takahashi [b], K. Minekawa [b], Y. Kawase [b,*]

[a] *Department and Engineering Research Center, Mizushima Plant, Mitsubishi Chemical Corporation, Kurashiki, Okayama 712-8054, Japan*

[b] *Department of Applied Chemistry, Research Center for Biochemical and Environmental Engineering, Toyo University, Kawagoe, Saitama 350-8585, Japan*

Received 13 December 2002; accepted 14 May 2003

Abstract

An experimental investigation into power consumption and solid suspension performance of large-scale impellers was carried out under turbulent conditions. Two types of large-scale impellers, i.e. Maxblend and Fullzone impellers, were employed. For reference, a triple-impeller system, i.e. two four-pitched blade downflow disk turbines (DTs) at middle and upper positions and one Pfaudler type impeller at lower position, was also used. The power consumption and the minimum impeller speeds for off-bottom solid suspension and minimum impeller speeds for ultimately homogeneous solid suspension were measured in unaerated and aerated systems.

At a given rotational speed, the power consumption of the Maxblend impeller was roughly half of that of the Fullzone impeller. The decrease in power consumption due to aeration for large-scale impellers was smaller as compared with that for the triple-impeller system. The proposed correlation for power consumption of large-scale impellers in three-phase systems fit the experimental data reasonably well.

Interesting and unexpected solid movements caused by the large-scale impellers in the vessels having oval bottom were observed. Since the large-scale impellers create strong axial liquid recirculation flowing downward near the impeller shaft and upward near the wall, usually particles are expected to move outward on the tank bottom. On the contrary, however, solid particles near the bottom moved to the center of the base from the side along the oval tank bottom.

The large-scale impellers were found to be more efficient for solid suspension than the triple-impeller system. The Maxblend impeller provided the best solid suspension ability among the three impellers used in this work. We proposed a correlation for power consumption of large-scale impellers in gas–liquid–solid three-phase systems. Empirical correlations were also proposed for the minimum impeller speeds for off-bottom solid suspension, minimum impeller speeds for ultimately homogeneous solid suspension and power consumption at the minimum impeller speeds for ultimately homogeneous solid suspension.

Keywords: Power consumption; Solid suspension; Large-scale impellers; Three-phase stirred tank

1. Introduction

Gas–liquid–solid three-phase stirred tanks have been frequently employed in the process industry and impeller design for three-phase operation is a challenging and industrially relevant task. The knowledge of the extent of the solid mixing is essential for the determination of overall rates of heat and mass transfer and reactions and consequently important in the design and scale-up of solid suspension mixing apparatus. It is clear that better understanding of the solid dispersion leads to the rational design and scale-up of gas–liquid–solid three-phase stirred tank reactors.

An appropriate choice of impellers, which always provide good mixing under varying hydrodynamic conditions, is of vital importance. In semi-batch operations, for example, the liquid level changes with time. In the case of polymerization at the batch operation, furthermore, reaction starts out in a low-viscosity medium like water and the viscosity of the reaction medium increases as polymerization proceeds. Hydrodynamic characteristics in stirred tank reactors change with time during the reaction process. Although helical ribbon and anchor impellers have been used industrially in polymerization reaction systems, they are sometimes ineffective with low-viscosity liquids at the beginning of polymerization processes. Recently, various large-scale impellers applicable over a wide range of hydrodynamic conditions have been developed particularly in Japan and extensively applied to the mixing operations in chemical and biochemical industries [1–3]. The Maxblend impeller developed by Sumitomo Heavy Industries Ltd., Japan, the Fullzone impeller developed by Shinko Pantec

* Corresponding author. Tel.: +81-49-239-1377; fax: +81-49-231-1031.
E-mail address: bckawase@mail.eng.toyo.ac.jp (Y. Kawase).

1385-8947/$ – see front matter © 2003 Elsevier B.V. All rights reserved.
doi:10.1016/S1385-8947(03)00148-7

Nomenclature

a–d	coefficients in Eq. (3)
C	impeller clearance (m)
C_s	solid concentration (vol.%)
D_I	impeller diameter (m)
D_p	particle diameter (m)
D_T	tank diameter (m)
Fr_g	Froude number for aeration $= U_g^2/D_I g$
Fr_N	Froude number $= N^2 D_I/g$
g	gravitational acceleration (m s^{-2})
h	width of impeller blade (m)
H	liquid height (m)
I	moment of inertia (kg m^2)
k	number of impeller blade
K	proportionality constant, Eq. (10)
m	proportionality constant, Eq. (13)
N	impeller speed (s^{-1})
N_{js}	critical impeller speed for just complete off-bottom solid suspension (s^{-1})
N_{jsg}	critical impeller speed for just complete off-bottom solid suspension under aeration (s^{-1})
N_{us}	minimum impeller speed for ultimately homogeneous solid suspension (s^{-1})
N_{usg}	minimum impeller speed for ultimately homogeneous solid suspension under aeration (s^{-1})
P	power consumption (W)
P_g	gassed power consumption (W)
P_{gv}	power consumption per liquid volume (W m^{-3})
P_{usg}	power consumption at N_{usg} (W)
R_1	distance between the center of shaft and the outer side of impeller blade (m)
R_2	distance between the center of shaft and the inner side of impeller blade (m)
S	proportionality constant, Eq. (4)
U_g	superficial gas velocity (m s^{-1})
U_t	terminal settling velocity of particle (m s^{-1})
V	liquid volume (m^3)
W_s	solid weight fraction

Greek letters

θ	inclination of impeller blade (rad)
μ_l	liquid viscosity (Pa·s)
$\mu_{l\,eff}$	effective liquid viscosity (Pa·s)
ν	kinematic viscosity (m^2 s^{-1})
$\Delta\rho$	density difference between particle and liquid (kg m^{-3})
ρ_l	liquid density (kg m^{-3})
$\rho_{l\,eff}$	effective liquid density (kg m^{-3})
ρ_s	solid density (kg m^{-3})
ϕ_s	solid volume fraction
ϕ'	characteristic angle (rad)
ω	angular velocity (rad s^{-1})

Co. Ltd., Japan, Hi-F Mixer developed by Soken Chemical & Engineering Co., Ltd., Japan and the Sanmeler impeller developed by Mitsubishi Heavy Industries Ltd., Japan, are typical examples of large-scale impellers [2]. The large-scale impellers consisting of modified large paddle impellers are versatile and applicable in not only rather low but also high Reynolds number regimes. Moreover, large-scale impellers are available to semi-batch operations in which the liquid level changes, since the ratio of (impeller height)/(impeller diameter) is large and the impeller bottom is very close to the tank base. In spite of their wide applicability, however, the performance of these impellers is not published in the open literature and still very indistinct. For optimal solid suspension, the design of impellers needs adequate off-bottom suspension and sufficient solids dispersion throughout the stirred tank reactor. Relatively less has been done in determining dispersion of solids through stirred tanks with large-scale impellers. In this work, therefore, we examined solid mixing characteristics over a wide range of hydrodynamic condition for the Maxblend impeller and the Fullzone impeller. The primary objective of the present investigation is to present novel findings and new data on solid suspension in stirred tank reactors with large-scale impellers. This paper focuses on two aspects which are critical to solid suspension: off-bottom solid suspension and uniform solid dispersion. We measured the minimum impeller speed for off-bottom solid suspension at which all particles are in motion and no particle remains on the tank bottom for more than one or two seconds. Under this so-called complete or off-bottom suspension, as described below in detail, most solid particles move in the solid particle pile formed on the tank bottom. This condition does not ensure that all the surface of the particles is available for heat and mass transfer and chemical reaction. Homogeneous solid suspension is often desirable for crystallization, polymerization, heterogeneous photocatalytic reaction, etc. [4]. Therefore, we also measured the minimum impeller speeds for ultimately homogeneous solid suspension defined as the speeds beyond which more uniform or homogenous solid suspension are not obtained.

2. Experimental

In order to examine the scale-up problem, experiments were carried out in five different scale vessels, 200, 310, 400, 600 and 800 mm i.d. The vessels are cylindrical and have oval bottom with four 0.08-width baffles. The distance between the tangent limit (TL: the transition point from the curved bottom to the vertical wall) and the stirred tank bottom is $D_T/2$. This rather large curvature of the tank bottom is common in the process industry. The liquid height in the tank, H, equaled tank diameter, D_T, for 200, 310, 600 and 800 mm i.d. tanks. For a 400 mm i.d. tank, the liquid height was $1.2D_T$. The schematic diagram of large-scale impellers used in this work, Maxblend impeller (Sumitomo Heavy Industries, Ltd., Japan) and Fullzone impeller (Shinko

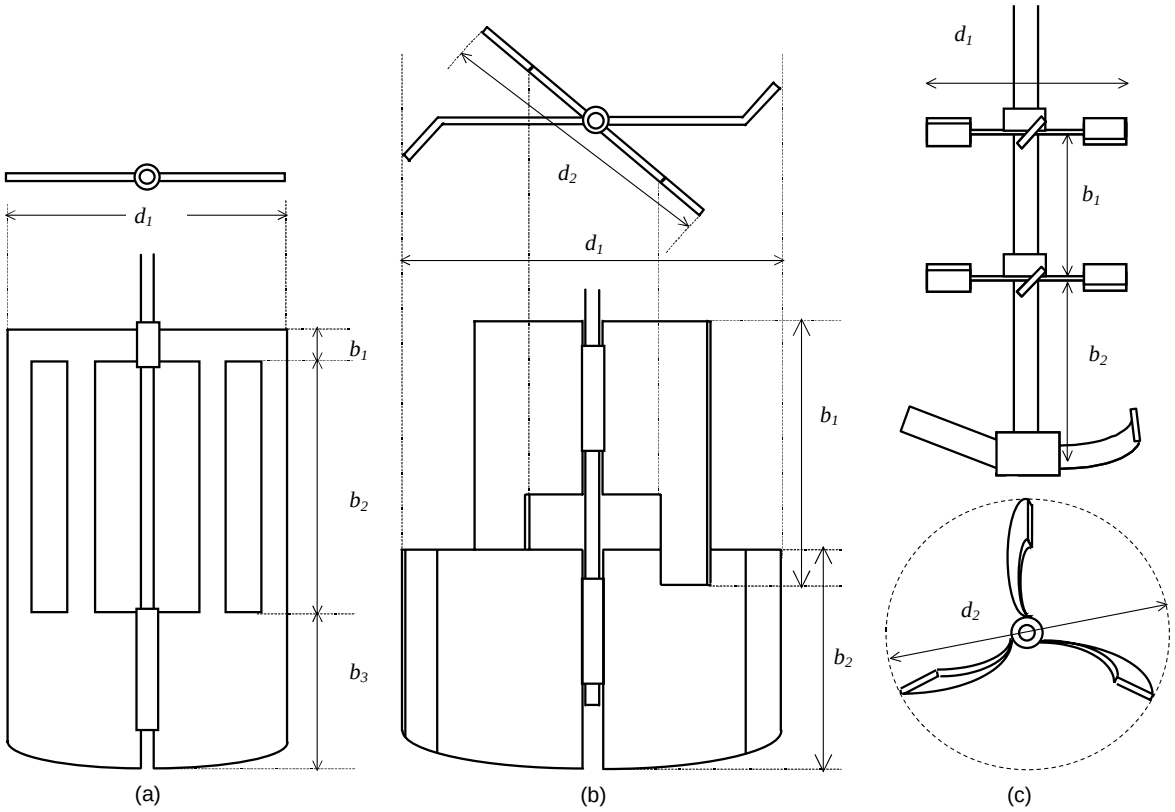

Fig. 1. Impellers used in this study: (a) Maxblend impeller, (b) Fullzone impeller, (c) triple-impeller system.

Pantec Co., Ltd., Japan) are illustrated in Fig. 1a and b. Many industrial stirred tanks are usually provided with multiple impellers mounted on the same shaft to satisfy a variety of mixing requirements. For comparison, therefore, we also used triple impellers, i.e. two four-pitched blade downflow disk turbines (DTs) at middle and upper positions and one Pfaudler type impeller at lower position. This configuration shown in Fig. 1c was used in our previous work [5]. The Pfaudler type impeller was installed to scrape solid particles on the oval bottom as close to the bottom as possible. Pertinent details of the impeller designs used in this work are summarized in Table 1.

The distance of the impeller from the tank bottom is very important for solid suspension and in the present work the tank diameter-to-impeller clearance ratios recommended by the impeller manufactures were used. The impeller clearance, C, was measured from the bottom of the impeller to the tank bottom. They are rather small to improve the off-bottom suspension. Air was used as gas phase and introduced through a ring sparger installed along the wall at the TL of the stirred tank. The ring sparger could not installed under the impeller due to considerably small impeller clearance. The gas flow rate was measured with a rotameter. The rotational speed of the impellers was varied by means of a variable-frequency drive. The impeller speed and gas velocity were varied from 1.25 to 13.3 s^{-1} and from 0.01 to 0.092 $m\,s^{-1}$, respectively. The corresponding range of the impeller Reynolds number was from 36,000 to 416,000. Since rather large power inputs or impeller speeds were required to move and suspend solid particles, flow conditions in the stirred tanks were turbulent. Tap water was used as liquid phase. Some additional data were also obtained

Table 1
Details of impeller designs

Tank i.d. (mm)	d_1/D_T	b_1/D_T	b_2/D_T	b_3/D_T	C/D_T
(a) Maxblend impeller					
ϕ200	0.53	0.43	0.650	0.33	0.05
ϕ310	0.53	0.43	0.607	0.33	0.05
ϕ400	0.53	0.43	0.833	0.33	0.05
ϕ600	0.53	0.43	0.563	0.33	0.05
ϕ800	0.53	0.43	0.616	0.33	0.05
	d_1/D_T	d_2/D_T	b_1/D_T	b_2/D_T	C/D_T
(b) Fullzone impeller					
ϕ310	0.60	0.55	0.6	0.43	0.05
ϕ400	0.55	0.50	0.6	0.45	0.05
(c) Triple-impeller system (two four-pitched blade downflow DTs and one Pfaudler type impeller)					
ϕ200	0.42	0.60	0.425	0.51	0.1
ϕ310	0.45	0.55	0.425	0.51	0.1
ϕ400	0.42	0.58	0.425	0.51	0.1
ϕ800	0.42	0.60	0.425	0.51	0.1

Table 2
Properties of glass beads

	Mean diameter (μm)
GA	187
GB	345
GC	560
GD	810

in relatively dilute aqueous solutions of glycerin (μ = 0.005–0.050 Pa·s). As solid particles, we employed four different size glass beads which had a density of 2500 kg m^{-3} (Table 2). The solid loading was varied from 0 to 30 vol.%. Experiments were performed in a semi-batch manner. Power consumption was measured using torque meters (Three-One Motor, Shinnto Sci. Co. and TS 3100B, Ono Sokki Co.).

The minimum impeller speeds for off-bottom solid suspension, N_{js} for solid–liquid two-phase systems and N_{jsg} for solid–gas–liquid three-phase systems, were determined using visual observations at bottom of the tank. Following Zwietering's definition of the minimum impeller speeds for off-bottom solid suspension [6], the impeller speeds when no particles remain longer than 1 or 2 s were defined as N_{js} or N_{jsg}.

The minimum impeller speeds for ultimately homogeneous solid suspension, N_{us} for solid–liquid two-phase systems and N_{usg} for solid–gas–liquid three-phase systems, were systematically determined using the plots of the volume fraction of solid particles in the sample taken from the bulk of the mixture against the corresponding impeller speed. Slurry samples were withdrawn from the bulk of a mechanically agitated and aerated mixture at different impeller speeds and gas flow rates using a small sampling tube. In the 0.80 m i.d. tank, for example, the distances of the three sampling points from the tank bottom were 0.44, 0.69 and 0.90 m, respectively, and their radial positions were 0.2 m from the tank wall. The sampling positions in other four tanks were equivalent to those in the 0.8 m i.d. tank, i.e. upper, middle and lower positions of liquid height near the center between the tank wall and impeller tip. As shown below, the volume fractions of the solids in the samples were determined and plotted as a function of the impeller speed at which they were obtained. In the resulting plots, the point at which a sharp change in the slope ended corresponds to ultimately homogeneous solids suspension. This method used for the determination of the minimum impeller speed for ultimately homogeneous solid suspension is similar to that used by many investigators [7–11]. Although the sample withdrawal method has shortcomings, as mentioned by MacTaggart et al. [8] it has been commonly and successfully used. As described below, when the homogeneous solid suspension was achieved, the solid volume fraction in the sample was nearly coincident with the average solid fraction, ϕ_s. This suggests that the sample withdrawal method used to determine N_{us} and N_{usg} in this work is reasonable. Of course replicated data were taken to ensure reliability of the experimental results.

3. Results and discussion

3.1. Power consumption

In order to correlate power consumption of the multi-impeller system in liquid single-phase and liquid–solid two-phase systems [5], we have successfully applied a moment model proposed by Mikamo [12] in which the energy required to rotate an impeller is calculated by estimating a moment of inertia of the impeller. In the present work, we extended the model to large-scale impellers. The resulting correlation may be written as:

$$P = \frac{1}{2} I\omega^3 = \frac{1}{8} h\rho_{l\,\mathrm{eff}}\phi' k(R_1^4 - R_2^4)\omega^3 \sin^2\theta \quad (1)$$

where the effective density for solid suspensions is given by

$$\rho_{l\,\mathrm{eff}} = \rho_s\phi_s + \rho_l(1-\phi_s) \quad (2)$$

Eq. (1) suggests that P is proportional to N^3 or ω^3 and this coincided with the experimental results. This fact supports the applicability of Eq. (1). The coefficient ϕ' in Eq. (1) depends on the impeller design and the values of ϕ' for the impellers used in this work are given in Table 3. As shown in Fig. 2, the experimental results for power consumption without aeration can be correlated by Eq. (1) reasonably well. It can be seen from Fig. 2 that the predictions for the Maxblend impeller in the single-phase system somewhat overestimated. We observed that the entrainment through the free surface was occurred only by the Maxblend impeller. The gas holdup due to gas entrainment through the free surface reduced the power consumption and as a result the power consumption data for the Maxblend impeller were smaller as compared with the predictions by Eq. (1) for single-phase systems. The four vertical slits on the Maxblend impeller (Fig. 1a) providing the path for strong downward axial flow along the impeller shaft were responsible for the gas entrainment through the free surface.

Fig. 3 represents the response of P_g/P to gas flow rate variations. The power consumption decreased due to aeration because of the formation of cavity behind the impeller blades. It is seen that the decrease in power consumption for large-scale impellers was smaller as compared with that for the triple-impeller system represented by a solid line. In

Table 3
Values of ϕ'

Impeller	ϕ'
Maxblend	$\pi/3$
Fullzone	$\pi/2$
DT-Pfaudler	
Four-pitched blade downflow DT	$3\pi/5$
Pfaudler type impeller	$5\pi/9$

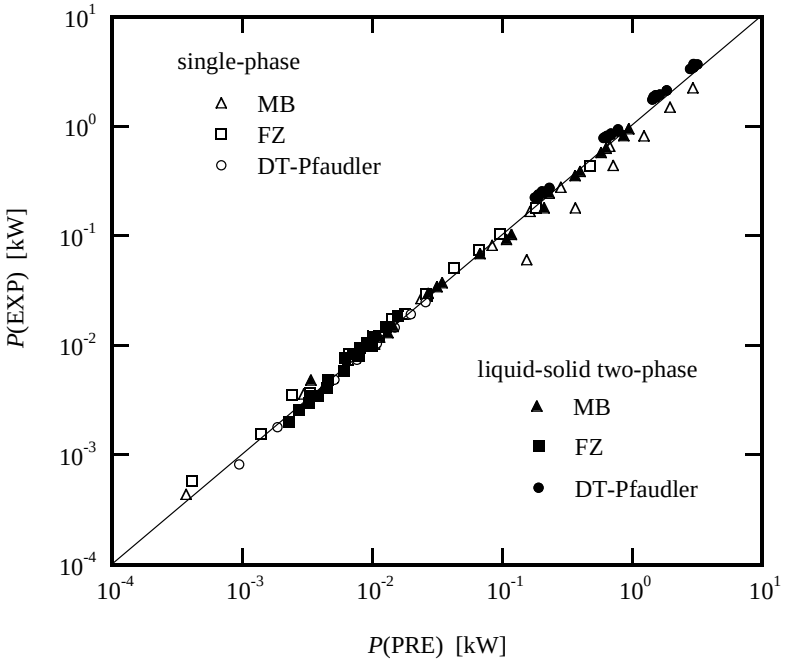

Fig. 2. Comparison for power consumption in liquid single-phase and liquid–solid two-phase systems between the experimental results and the predictions of Eq. (1) ($D_T = 400$ mm).

gas–liquid two-phase systems, we observed that the cavities formed behind the large-scale impellers were rather smaller than those behind the triple-impeller system.

For power consumption in gas–liquid–solid three-phase systems, we derived the following empirical correlation in the dimensionless form:

$$\frac{P_{gv}}{\rho_{l\,eff} g U_g} = a Fr_g^b Fr_N^c \left(\frac{D_I}{D_T}\right)^d \quad (3)$$

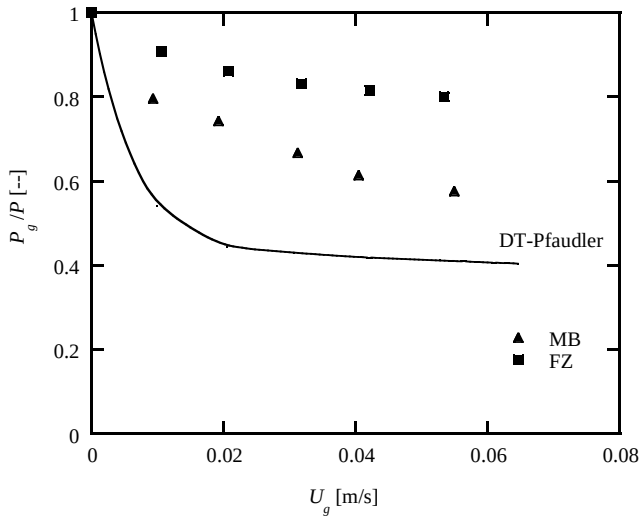

Fig. 3. Effect of aeration on power consumption ($D_T = 400$ mm, $N = 200$ rpm, $\phi_s = 0.2$, Glass beads: GA).

The coefficients *a–d* for the impellers used in this work are presented in Table 4. It can be seen in Fig. 4 that Eq. (3) fits the experimental data satisfactorily.

3.2. Visual observation of solid suspensions

The flow pattern generated in a stirred tank is the result of the geometrical configurations of the impeller and tank, the liquid properties, the gas flow rate and the rotational impeller speed and is responsible for the quality of mixing. The solid suspension occurs mainly because of the liquid flow induced by the impeller. Therefore, the overall liquid flow in the stirred tank was visually observed by the discoloration technique involving the redox reaction between iodine and sodium thiosulfate [13]. This technique has been widely used for measurement of mixing time and it is useful to look at overall liquid flow pattern in stirred tank. The particle motion was also visually observed through the transparent tank walls and tank bottom.

The flow produced in a stirred tank was strongly dependent on the impeller geometry and the shape of the tank bottom. As depicted in Fig. 1a, the Maxblend impeller is a single paddle impeller having four vertical slits on its

Table 4
Coefficients *a–d* in Eq. (3)

Impeller	*a*	*b*	*c*	*d*
Maxblend	0.32	−0.55	1.43	−0.55
Fullzone	0.55	−0.55	1.43	−0.55
DT-Pfaudler	0.023	−0.58	1.50	−0.58

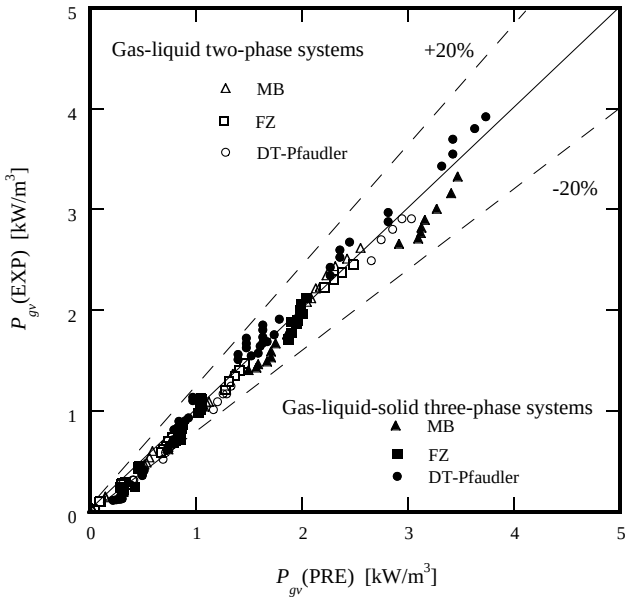

Fig. 4. Comparison for P_{gv} in gas–liquid two-phase and gas–liquid–solid three-phase systems between the experimental results and the predictions of Eq. (3) ($D_T = 400$ mm).

upper part. The lower part is a large paddle impeller and created strong radial liquid flows converted to strong axial upward-flows near the tank wall by the configurations of oval bottom and tank wall. The large-scale impellers were usually placed with a small clearance from the bottom. At the free surface, the liquid flow changed direction and went towards the impeller shaft. Again it changed direction and spirally flowed downward along the shaft to the bottom. The slits on the upper part drew in liquid flows and created rather defined downflows along the shaft.

As shown in Fig. 1b, the Fullzone impeller consists of two large paddle impellers and the upper paddle is shifted at 45° in the rotating direction. As well as the Maxblend impeller, the liquid flow pattern with the Fullzone impeller was characterized by a global axial recirculation. The lower paddle with bent tips drove significant radial flows converted to strong axial upflows along the tank. The liquid flows traveling up away from the tank base changed direction at the free surface and flowed downward to the bottom. There was a rapid downflow along the shaft axis. The shift of two-impellers, upper and lower paddle impellers, enhanced downflow spiraled along the shaft.

In the triple-impeller system presented in Fig. 1c, the Pfaudler type impeller was installed exclusively to accomplish off-bottom suspension of solid particles, while the two four-pitched blade downflow DTs were chosen to provide good gas dispersion rather than good solid suspension. The four-pitched blade downflow turbine, for which the angle of pitch is 45°, created axial downflow besides radial flow. Therefore, it is suitable for dispersion of bubbles formed at a sparger located below the impeller. The Pfaudler type impeller was installed to scrape solid particles on the oval bottom as close to the bottom as possible. As shown in Fig. 1c, the blades of the Pfaudler type impeller were angled to create downflow for good solid suspension and its design was suitable particularly for concave bottoms rather than flat bottoms.

We observed the interesting and unexpected movement of solid particles. The off-bottom suspension mechanism was controlled by the combination of solid movement and liquid flow adjacent to the tank bottom. On the whole, the liquid stream going to the bottom might be responsible for solids suspension. Since the minimum impeller speed for off-bottom solid suspension was taken as the rotational speed at which no particles are visually observed to remain at rest on the stirred tank bottom for more than 1 or 2 s, N_{js} and N_{jsg} largely depended on the local liquid flow in the vicinity of the tank bottom. At low impeller speeds, the majority of the particles rested on the bottom. We observed a stagnant spot of particles in the center of the bottom. The lower parts of the large-scale impellers were immersed into the solid particle pile. Consequently, solid particles in the peripheral ring region were pushed by the impeller and moved to the periphery with the impeller. As impeller speed increased, we observed two regions on the bottom, a center circle region and an outer annular ring region. The diameter of the center circle was about the diameter of the impeller. Most particles in the pile moved in the circumferential direction with the impeller. The particles in the upper part of the pile were swept to the periphery by the centrifugal force of the impeller immersed in the pile. A part of solid particles moved to the periphery were suspended by the upward liquid flow along the tank wall as described below. Another part of solid particles were retained in the pile, discharged from the surface to the bottom of the solid layers and moved to the center on the oval base. The solid particles, which were not lifted, recirculated inside the pile. On the whole the solid particles moved outwards on the surface of the pile but inwards on the base of the pile. The local liquid flow depended on the configuration of the tank bottom and the impeller clearance from bottom. We [14] have simulated the liquid single-phase flow in the oval bottom tank stirred by the Maxblend impeller using a commercial CFD software package, R-Flow (R-Flow Co., Japan). The simulation results for the velocity profiles in the 400 mm i.d. stirred tank with water suggest that there are strong liquid recirculation loop described above and significant streams flowing from the wall to the center of the tank bottom along to the oval tank bottom (Fig. 5). This result provides indirect evidence for particle motion observed near the tank bottom in the present work. Particles adjacent to the bottom moved to the center of the base from the side by the inward liquid flow and the gravitational force exerted on the particles. The general trends found in the literature are the opposite of the findings in this work. This difference might be due to the recirculation loop generated by the large-scale impellers, the curved shape of the tank bottom and the rather small impeller clearance used in this work ($C = D_T/20$). In most of the previous

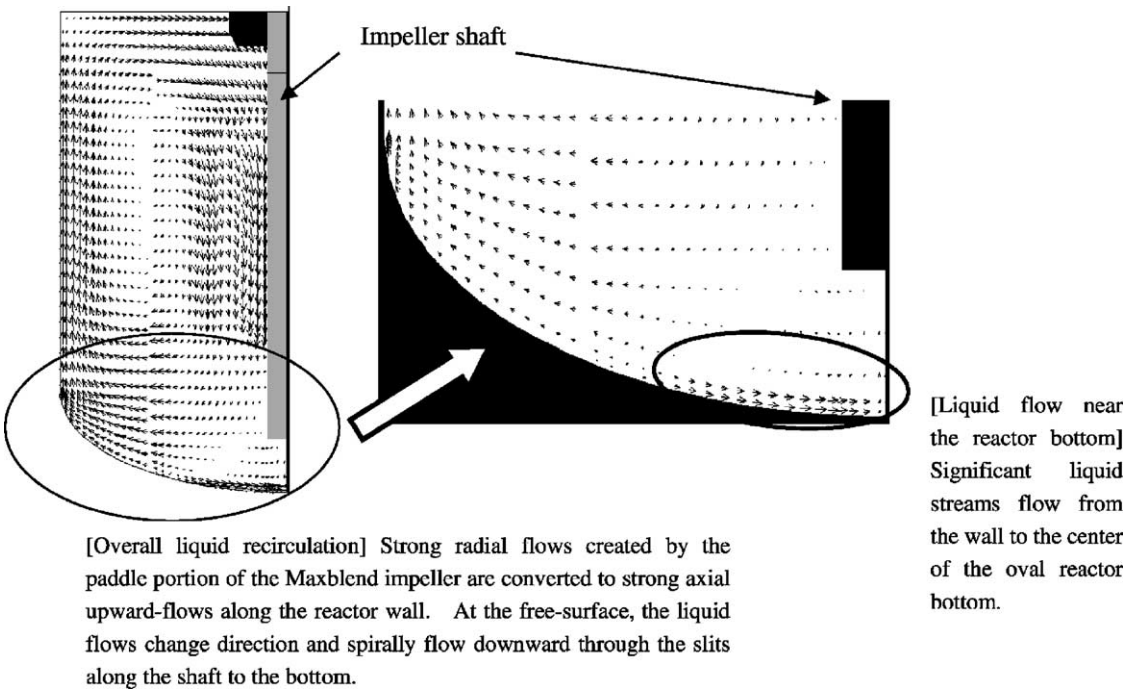

Fig. 5. Velocity vectors in a vertical plane at 45° between two baffles (bidimensional cross-section across the impeller shaft: only half-section shown; CFD simulation for Maxblend impeller in 400 mm i.d. stirred tank with water at $N = 150$ rpm).

investigations in which down-pumping axial impellers being the most efficient for solid suspension were used, the tank bottom was flat and the impeller clearance was rather large ($C = D_T/3$). Solid particles were swirled inwards in the center circle and chaotically moved in the annular ring. With an increase in impeller speed, the fluid flowing outwards increased and as a result the outward discharge of the particles was enhanced in the annular ring region. At higher impeller speeds, chaotic motion of solid particles was considerable enhanced and unstable eddies were observed as secondary streams of particles in the outer annular ring region. It should be noted that a similar movement of solid particles on the tank bottom was also observed with the Pfaudler type impeller.

The homogeneous suspension mechanism was governed by the bulk liquid recirculation unlike the complete or off-bottom suspension mechanism [11]. The particles were lifted from the solid particle pile or solids layer formed on the bottom by the recirculation flows. The particles were picked-up from the surface of the solid particle pile near the wall where strong radial liquid flows converted to strong axial upward-flows. For the large-scale impellers, as described above, they induced strong axial circulations flowed downward around the impeller shaft, outwards to the wall near the bottom and turned upwards along the wall. The particles lifted from the solid particle pile were transported to the top of the tank by induced recirculation loop. The liquid motion over the particles pile had a significant sweeping action from the center towards the outside. At low impeller speeds, particles were partially suspended and the majority of the particles rested on the bottom. The solid concentration near the bottom was relatively high while the upper and middle regions of the tank had rather low particle holdups. As impeller speed was increased, the particles were rapidly suspended through the stirred tank. When the impeller speed was increased, more and more particles were suspended from the surface of the solids layer formed on the tank bottom. The solid concentration near the bottom was drastically reduced and the concentrations of the samples taken from the middle and upper levels of the tank increased.

3.3. Off-bottom solid suspension

In Fig. 6, the variation in the minimum impeller speeds for off-bottom solid suspension for liquid–solid two-phase systems in the stirred tank of 400 mm i.d., N_{js}, with respect to solid particle diameter, D_p, is illustrated. With an increase in D_p, N_{js} increased as well as the results reported by Raghava Rao et al. [15]. Higher liquid flow rate was required to suspend the larger particles. It can be seen that N_{js} for the triple-impeller system was twice as much as larger than for the large-scale impellers. It may be concluded, therefore, that the large-scale impellers are more efficient for solids suspension than the triple-impeller system. The effect of solid volume fraction is also included in this figure. Values of N_{js} slightly increased with an increase in solids loading. It may be related to the fact that an increase in solids loading reduced the liquid flow generated by impeller for a given D_p. The suspended particles damped the turbulence by dissipating some energy around them [15].

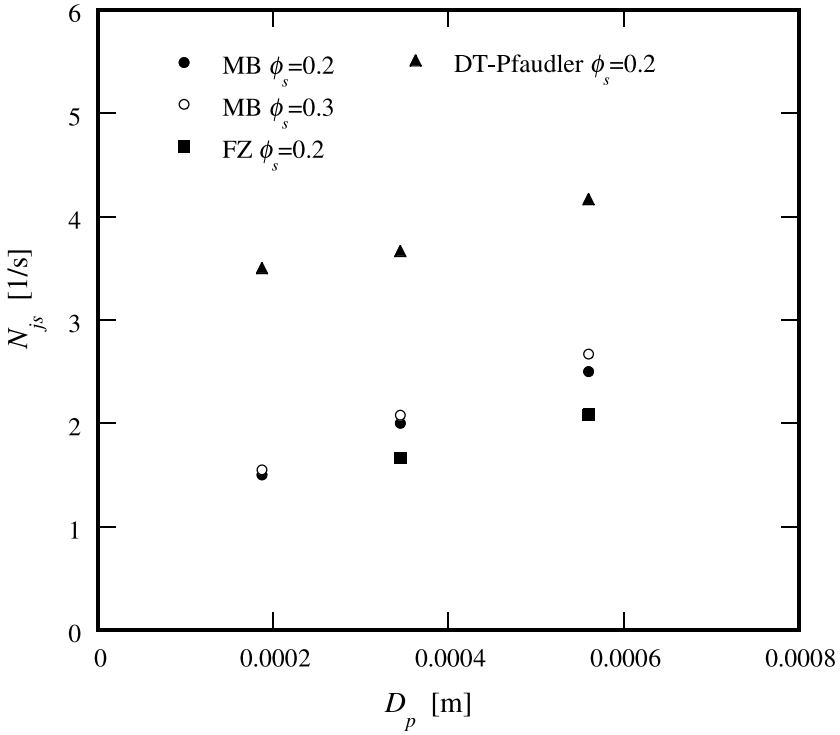

Fig. 6. Effect of particle size on N_{js} ($D_T = 400$ mm).

In order to correlate N_{js}, we obtained the following equation based on Zwietering's correlation [6]:

$$N_{js} = \frac{S\nu^{0.1}(g\Delta\rho/\rho_l)^{0.45}D_p^{0.2}W_s^{0.13}}{D_I^{0.85}} \quad (4)$$

where the weight fraction of solids, W_s, is related to the volume fraction of solids, ϕ_s, as

$$W_s = \frac{\rho_s\phi_s}{\rho_l(1-\phi_s)+\rho_s\phi_s} \quad (5)$$

The parameter S in Eq. (4) is a function of impeller type and system geometry. Although, as described above, the motion of solid particles on the tank base observed in this work was different from the particle motion reported in the literature, the values of the exponents in Eq. (4) did not change with the impeller designs and there was a change only in the proportionality constant. Values of S for the Maxblend and Fullzone impellers were nearly indistinguishable from each other and 3.2. The parameter S for the triple-impeller system was 6.5. It is seen in Fig. 7 that Eq. (4) corresponds to the experimental results for the Maxblend impeller, Fullzone impeller and triple-impeller system, respectively. The average regression correlation coefficient is 0.871. It is clear from the values of S obtained in this work that large-scale impellers require much lower impeller speed than that of small-scale impellers in order to make complete off-bottom solid suspension. Furthermore, considering the value of S in Eq. (4) for a DT ($D_I/D_T = 1/3$ and $C/D_T = 1/4$) is 8 and that for a propeller is 6.6 [16], it may be concluded that the large-scale impeller design has a significant advantage compared with the traditional design.

Aeration of the liquid–solid suspension resulted in a slight increase of the minimum impeller speed for off-bottom solid suspension for all the impellers. As gas rate increased, the power input decreased. Therefore, a higher impeller speed was necessary to move solid particles under aerated conditions than unaerated. Introduction of a gas also led to a decrease liquid flow flowing down to the tank base and as a result decayed the solid suspension ability of the impellers. This slight change in this work is related to the fact that, as stated previously, the ring sparger was located above the bottom end of the impellers, leading to only a little decrease in the impeller solids suspension performance. In the aerated systems, as well as the unaerated systems, the large-scale impellers were more efficient for solids suspension than the triple-impeller system.

We have developed the following empirical correlation for N_{jsg} in the gas–liquid–solid three-phase systems using the present data:

$$N_{jsg} = N_{js}\left(1 + 0.03\left(\frac{U_g}{U_t}\right)^{0.2}Re_p^{0.4}\right) \quad (6)$$

where

$$Re_p = \frac{D_pU_t}{\mu_{l\,eff}/\rho_{l\,eff}} \quad (7)$$

$$\mu_{l\,eff} = \mu_l\frac{1+0.823\phi_s^5}{1-2.478\phi_s+18.456\phi_s^5-20.326\phi_s^6} \quad (8)$$

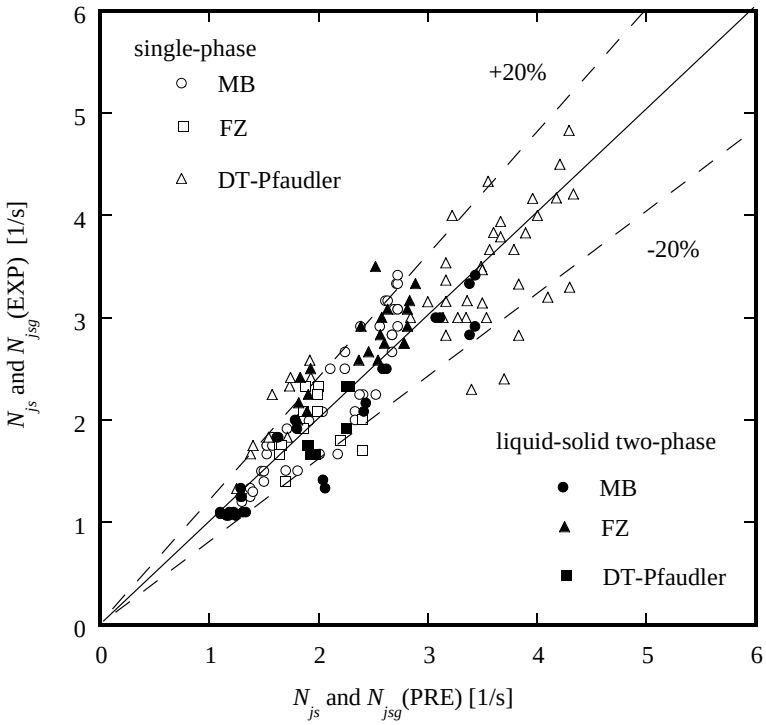

Fig. 7. Comparison between the experimental results for N_{js} and N_{jsg} and the predictions of Eqs. (4) and (6).

$$U_t = \frac{(\rho_s - \rho_l) g D_p}{\{18\mu_l + D_p^{1.5}(2.335 - 1.774\phi_s)\rho_l^{0.5}(\rho_s - \rho_l)^{0.5} g^{0.5}\}} \quad (9)$$

In Eq. (6), the terms of (U_g/U_t) and Re_p were introduced to consider the effects of aeration and sedimentation characteristics of solid particles on the critical impeller speed for solid suspension, respectively. The terminal settling velocity of particle in slurries, U_t, is estimated by the equation presented in the book of Kunii and Levenspiel [17] and the effective viscosity for slurries, $\mu_{l\,eff}$, is evaluated using the theoretical correlation derived by Kawase and Ulbrecht [18]. Fig. 7 also compares the prediction of Eq. (6) and the present experimental results for gas–liquid–solid three-phase systems. Reasonable agreement can be found with the correlation coefficient of 0.845.

3.4. Ultimately homogeneous solid suspension

Typical data for solid concentrations in the stirred tanks are illustrated in Fig. 8. At lower impeller speeds, the majority of the solid particles rested on the tank bottom. As impeller speed increased, the solid particles were rapidly suspended through the tank. A sharp change in the slope of the curve for solid volume fraction in the sample, C_s, as a function of impeller speed occurred. Following this sharp change in slope, curves began to approach the plateau. In other words, as the impeller speed increased the solid concentrations leveled off and approached the ultimate solid dispersion. It should be noted that the solid volume fraction in the sample was nearly coincident with the average solid fraction, ϕ_s, when the homogeneous solid suspension was achieved. An estimation of N_{us} and N_{usg} was obtained as the impeller speed in correspondence to the sharp change in slope of solid volume fraction-impeller speed plot. It can be seen from Fig. 8 that the impeller speed at a sharp change in the slope of the curve for C_s vs. N increased with increasing U_g.

The effect of particle size on N_{us} in the stirred tank of 400 mm i.d. is shown in Fig. 9. With an increase in particle size the settling velocity increased and therefore higher average liquid velocity created by the impeller was required to suspend the solid particles. As a result, values of N_{us} increased with an increase in D_p. For all the impellers, a similar dependence of N_{us} on D_p was found. The effect of solids loading is also shown in Fig. 9. With an increase in solids loading N_{us} slightly increased. This may be related to the fact that some of the impeller energy dissipated at the solid–liquid interface and the liquid recirculation flow rate decreased with increasing solids loading.

Fig. 10 shows typical values of N_{usg} against the superficial gas velocity for $D_p = 342\,\mu m$ (Glass beads GB) and $\phi_s = 0.2$. It is seen that N_{usg} depended on the gas flow rate. The critical impeller speed for ultimately homogeneous solid suspension in the presence of gas was found to be more than that in the absence of the gas. The decrease in power input resulted from cavity formation behind the impeller led to an increase in the critical impeller

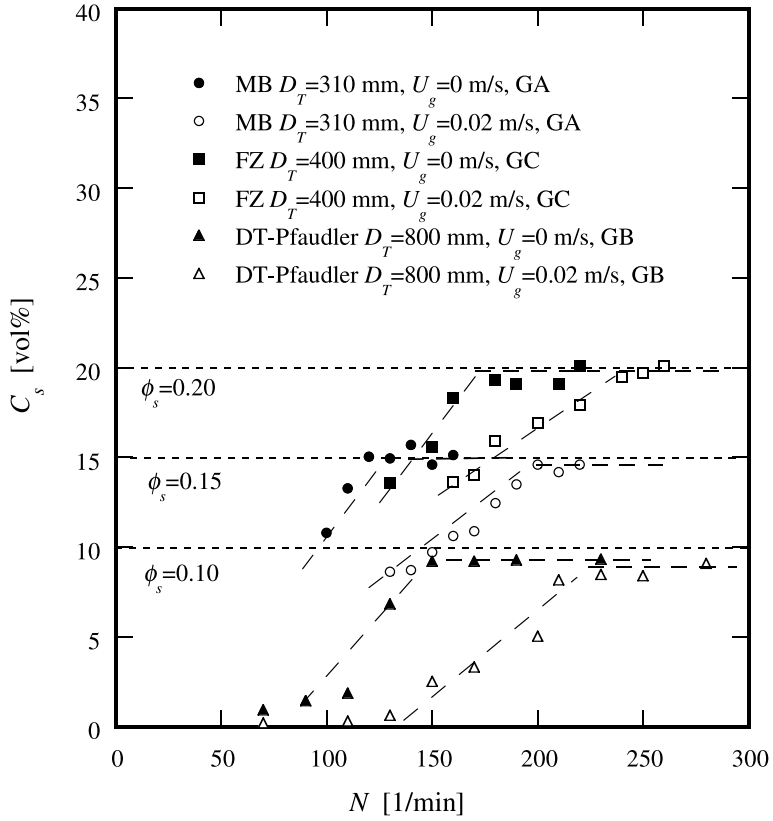

Fig. 8. Typical solid concentrations in the sample taken from the bulk of the tank at the middle sampling point (MB: $\phi_s = 0.15$, FZ: $\phi_s = 0.20$, DT-Pfaudler: $\phi_s = 0.10$).

speed for ultimately homogeneous solid suspension. In addition, the downward liquid flows generated by impeller, which are effective at lifting solids, were damped out by aeration. Aeration has more influence on N_{usg} as compared with that on N_{jsg}. The effect of stirred tank size has been also included in Fig. 10. With decreasing tank diameter, the value of N_{usg} increased. The dependence of N_{usg} on U_g for all the impellers could be considered essentially the same in-as-much as the range of U_g examined in this work.

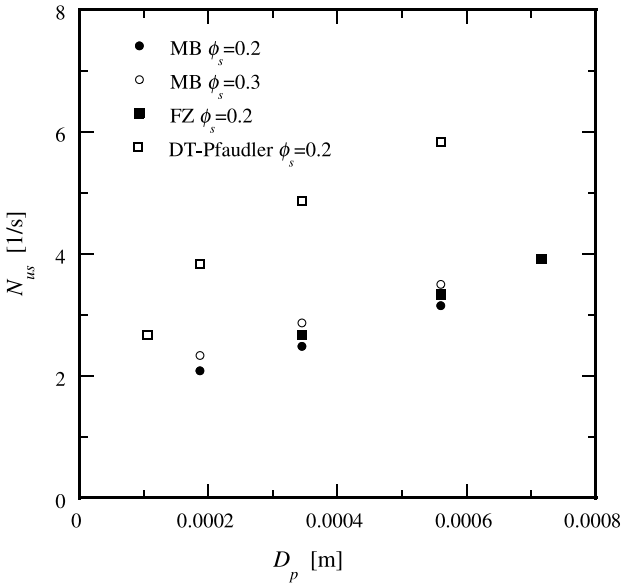

Fig. 9. Effect of particle size on N_{us} ($D_T = 400$ mm).

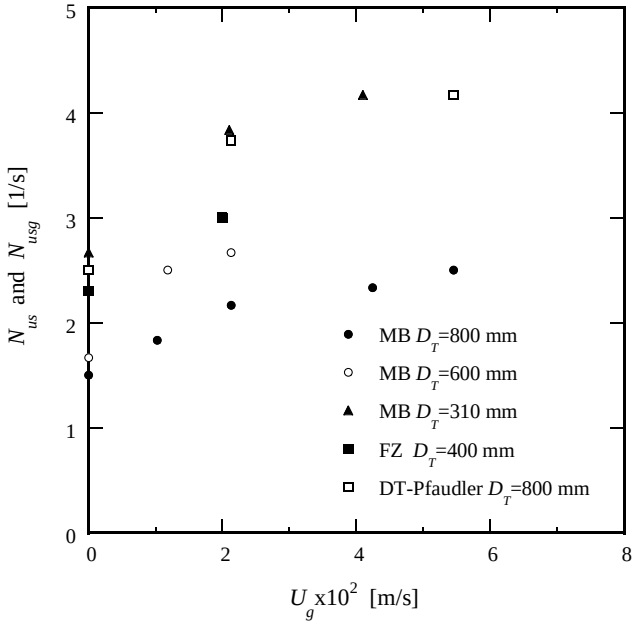

Fig. 10. Effect of gas flow rate on N_{usg} ($\phi_s = 0.2$, Glass bead: GB).

We developed the following empirical correlation for N_{us}:

$$N_{us} = \frac{K\nu^{-0.25}(g\Delta\rho/\rho_l)^{0.40}D_p^{0.47}W_s^{0.22}}{D_I^{0.80}} \quad (10)$$

Linear regression analysis on the data gave values for the proportionality constant K of 0.13, 0.15 and 0.28 for the Maxblend impeller, Fullzone impeller and the triple-impeller system, respectively. In the same way as N_{js} or N_{jsg}, the K values for large-scale impellers were less than a half as compared with that of the triple-impeller system leading the fact that the large-scale impellers could make ultimately homogeneous solid suspensions at lower impeller speeds than that of the triple-impeller system. In the triple-impeller system, the two four-pitched blade downflow DTs discharged fluid in axial direction as well as the Maxblend and Fullzone impellers but the intensity of the discharge flow might be weak as compared with the large-scale impellers. A parity plot comparing the experimental results for N_{us} values and those predicted using Eq. (10) is depicted in Fig. 11. The predictions of Eq. (10) are in reasonable agreement with the present experimental data and the correlation coefficient is 0.836.

The above correlation was modified to extend to gas–liquid–solid three-phase systems as:

$$N_{usg} = N_{us}\left(1 + \frac{U_g}{U_t}\right)^{0.15} \quad (11)$$

Fig. 11 also shows the comparison between predictions from Eq. (11) and experimental results for N_{usg}. The correlation coefficient is 0.894. The predictions correspond reasonably well in both unaerated and aerated cases.

The power consumption when the impeller speed runs at N_{us} or N_{usg} can be written as follows:

$$\frac{gU_t}{P/(\rho_l V)} \propto \text{const} \quad (12)$$

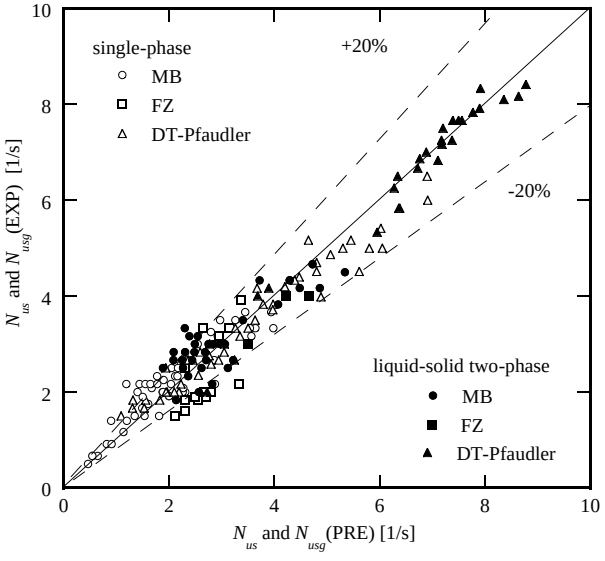

Fig. 11. Comparison between the experimental results for N_{us} and N_{usg} and the predictions of Eqs. (9) and (11).

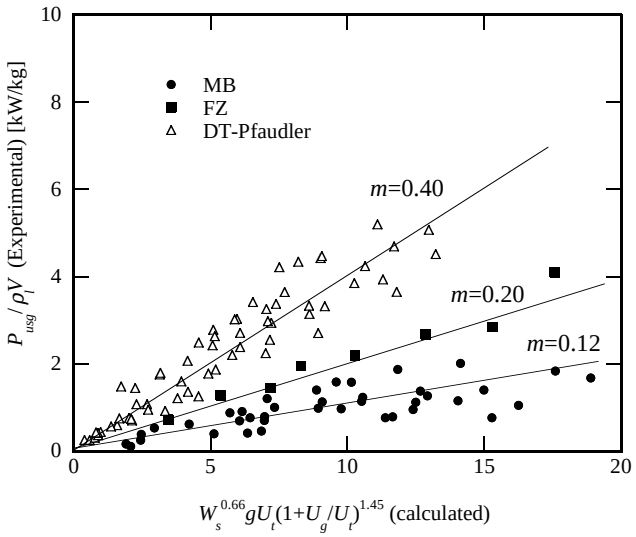

Fig. 12. Estimation of the constant m in Eq. (13).

This equation is composed of particle motion energy (numerator) and energy dispersion rate (denominator). Based on this relationship, we developed an empirical correlation for P_{us} and P_{usg} defined as the energy dispersion rate at N_{us} and N_{usg}, respectively, as follows:

$$\frac{P_{usg}}{\rho_l V} = mW_s^{0.66} gU_t\left(1 + \frac{U_g}{U_t}\right)^{1.45} \quad (13)$$

The performance comparison for uniform solid suspension among the impellers is presented in Fig. 12. When the constant m was determined as 0.12, 0.20, and 0.40 for the Maxblend impeller, Fullzone impeller and triple-impeller system, respectively, Eq. (13) fit the experimental results reasonably well. Supposed from this fact, it was found that the power consumptions for uniform solid suspension of large-scale impellers were much lower than those of small-scale impellers. As shown in Fig. 9, the values of N_{us} for the Maxblend and Fullzone impellers were nearly indistinguishable from each other as long as N_{us} values were plotted against D_p. It is clear from Fig. 12, however, that the P_{vus} values for the Maxblend impeller were about a half smaller than those for the Fullzone impeller. This is due to the fact that the power consumption of the Fullzone impeller was about 30% larger than that of the Maxblend impeller at the same impeller speed. Whereas, as described above, the Fullzone impeller consists of two large paddle impellers, the Maxblend impeller has four vertical slits on their upper parts of a paddle impeller and therefore its power consumption is smaller as compared with that of the Fullzone impeller. The Maxblend impeller is more economical to achieve uniform solids suspensions. as compared with the Fullzone impeller. The Maxblend impeller is the best performer for uniform solid suspension among the impellers examined in this work.

4. Conclusions

We have experimentally examined power consumption and solid suspension performance of large-scale impellers, the Maxblend and Fullzone impellers in the turbulent flow regime.

At a given rotational speed, the power consumption of the Maxblend impeller was about half of that of the Fullzone impeller and the decrease in power consumption due to aeration for large-scale impellers was smaller than that for the triple-impeller system. The proposed correlation for power consumption of large-scale impellers in three-phase systems agreed reasonably with the experimental results.

Very interesting solid movements have been observed. Overall, particles adjacent to the bottom moved to the center of the base from the side. In the solid particle pile formed on the tank bottom, particles moved inwards very close to the tank base whereas near the surface of the pile they were pushed to the side. This finding for solid particles near the tank bottom is contrary to the general trends in the literature. The difference is associated with the curved shape of the tank bottom and the rather small impeller clearance. Suspension occurred from an annual ring on the solid particle pile. The liquid recirculation flow created by the large-scale impellers was very effective at lifting particles. As the solid particles were lifted, they were transported to the free surface by primary and induced recirculation loops. It may be concluded that the Maxblend impeller is the most favorable for more uniform solid suspension among the impellers used in this work. We have developed empirical correlations for the estimation of N_{jsg}, N_{usg} and P_{usg}. This study focuses on solid suspension in the turbulent regime. At next stage, solid-suspension performance of large-scale impellers in the transitional and laminar regimes will be examined. This work was undertaken as a starting point for systematic studies on performance of large-scale impellers.

References

[1] K. Yamamoto, K. Abe, A. Tarumoto, K. Nishi, M. Kaminoyama, M. Kamiwano, J. Chem. Eng. Jpn. 31 (1998) 335–365.
[2] K. Asano, in: Proceedings of the Third International Symposium on Mixing in Industrial Processes, Osaka, 1999, pp. 85–90.
[3] K. Takada, H. Itoh, M. Kikuchi, Y. Okamoto, Kagaku Kougaku Ronbunshu 25 (1999) 253–257.
[4] G. Micale, G. Montanye, F. Grisafi, A. Brucato, J. Godfrey, Trans. Inst. Chem. Eng. A 78 (2000) 435–444.
[5] N. Dohi, Y. Matsuda, N. Itano, K. Shimizu, K. Minekawa, Y. Kawase, Chem. Eng. Commun. 171 (1999) 211–229.
[6] T.N. Zwietering, Chem. Eng. Sci. 8 (1958) 224–253.
[7] J.R. Bourne, R.N. Sharma, Chem. Eng. J. 8 (1974) 243–250.
[8] R.S. MacTaggart, H.A. Nasr-El-Din, J.H. Masliyah, Chem. Eng. Sci. 48 (1993) 921–931.
[9] P.M. Armenante, Y.-T. Huang, T. Li, Chem. Eng. Sci. 47 (1992) 2865–2870.
[10] A.H.P. Skelland, N.M. Hassan, Chem. Eng. Sci. 54 (1999) 4273–4284.
[11] N. Dohi, Y. Matsuda, N. Itano, K. Minekawa, T. Takahashi, Y. Kawase, Can. J. Chem. Eng. 79 (2001) 107–111.
[12] M. Mikamo, Power consumption in the stirred vessel, MS Thesis, Hosei University, Tokyo, 1994.
[13] N.N. Dutta, V.G. Pangarkar, Can. J. Chem. Eng. 73 (1995) 273–283.
[14] T. Takahashi, N. Dohi, Y. Kawase, Can. J. Chem. Eng., in press.
[15] K.S.M.S. Raghava Rao, V.B. Rewatkar, J.B. Joshi, AIChE J. 34 (1988) 1332–1340.
[16] A.W. Nienow, Mixing in the Process Industries, Butterworths, London, 1985.
[17] D. Kunii, O. Levenspiel, Fluidization Engineering, 2nd ed., Wiley, New York, 1996.
[18] Y. Kawase, J.J. Ulbrecht, Chem. Eng. Commun. 20 (1983) 127–136.